

Jonathan L. du Bois¹
Department of Aerospace Engineering,
University of Bristol,
Queens Building,
University Walk,
Bristol BS8 1TR, UK
e-mail: jon.dubois@bristol.ac.uk

Sondipon Adhikari
Chair of Aerospace Engineering
School of Engineering,
Swansea University,
Singleton Park,
Swansea SA2 8PP, UK
e-mail: s.adhikari@swansea.ac.uk

Nick A. J. Lieven
Dean of Faculty of Engineering
University of Bristol,
Queens Building,
University Walk,
Bristol BS8 1TR, UK
e-mail: nick.lieven@bristol.ac.uk

On the Quantification of Eigenvalue Curve Veering: A Veering Index

Eigenvalue curve veering is a phenomenon that has found relevance and application in a variety of structural dynamic problems ranging from localization and stability studies to material property determination. Contemporary metrics for quantifying veering can be ambiguous and difficult to interpret. This manuscript derives three normalized indices in an effort to reconcile the deficit; two of these quantify the physical conditions which produce the behavior while the third provides a definitive measure of the overall intensity of the effect. Numerical examples are provided to illustrate the application of the methods, which are expected to form a basis for the development of advanced analytical tools. [DOI: 10.1115/1.4003189]

1 Introduction

The phenomenon of curve veering in eigenvalue loci has been observed in structural dynamics since detailed parametric studies began appearing in the 1960s, for example, Refs. [1,2]. With the advent of modern computational power, examples of the behavior now frequently appear in the literature. The first explicit experimental demonstration was given in Refs. [3,4], which also offer some historical background on the subject.

Principally, the description is applied to systems where two eigenvalue loci approach each other closely and suddenly veer away again, each one taking on the trajectory of the other. All of the properties of the two modes are swapped, including damping ratios, sensitivities, and eigenvectors (or eigenfunctions). The transition is always smooth, albeit abrupt, and will be shown to be an extreme manifestation of normal parametric variation. The effect is exploited by techniques for establishing the Poisson's ratio of orthotropic plates [5], plays a role in localization [6–9], and can be used in flutter prediction [10]. Its use has been advocated for analytical model updating [11] and damage detection [12], and its presence can have a strong influence on dynamic response in systems with sensitive configurations [13]; in uncertain systems, it has been observed that the marginal [14] as well as the joint probability density functions [15] of the eigenvalues can change significantly near the veering range.

Eigenvalue veering is a subset of a larger group of effects caused by modal interactions, also encompassing frequency coalescence and mode shape localization. Perkins and Mote [16] discussed the different behaviors of converging eigenvalue loci, which may veer away, veer with one another, attract one another before coalescing, or simply cross one another following locally independent trajectories. Triantafyllou and Triantafyllou [17] used complex analysis to present an alternative perspective on a range of modal interactions. Afolabi [18] applied catastrophe theory to linear vibrations to describe the nature of these behaviors. He also

distinguished between the resulting *geometric* and *elastic* instabilities, where the former is associated with curve veering and results in localization, and the latter is associated with coalescence and results in flutter instability. Seyranian and Mailybaev [19] used perturbation theory to explore modal interactions, focusing primarily on the so-called elastic stability conditions in the presence of eigenvalue coalescence. They went on to develop a comprehensive theory of eigenvalue interaction and the reader is referred to recent papers in collaboration with Kirillov in Refs. [20,21]. In the field of structural optimization, the occurrence of eigenvalue coalescence can be problematic and Seyranian et al. [22] provided numerous references to studies in this area.

This paper limits its scope to conservative self-adjoint systems, where it will be seen that the interaction of two modes will always lead to veering away of the eigenvalue loci. The limiting case of no modal interaction produces intersecting loci but as noted by other authors (for a recent example, see Ref. [23]), real world problems will never produce the perfect conditions required for this behavior.

The problem of quantifying veering was historically made difficult by the subjective nature of its identification. Its most tangible characteristic is the eigenvalue curvature or second derivative. Liu [24] suggested using critical values of the curvature or of the eigenvector derivatives to classify veering but conceded that the determination of these values would remain subjective. Perkins and Mote [16] derived “coupling factors” that they used to identify the expected behavior of converging modes; these factors provide great qualitative insight but quantitative interpretation can be misleading.

The remainder of the literature cited above uses a known intersection of multiple eigenvalue loci as a basis for describing the behavior of the modes. In contrast, this paper is concerned with the identification of veering with no prior knowledge of the system being studied. For this purpose, a nondimensional approach is taken to provide universal identification of the behavior. The method is based upon physically meaningful quantities and will indicate the presence of veering even where limited range or atypical context may obfuscate it. Sections 2 and 3 examine some important characteristics of veering modes, which are applied in Secs. 4 and 5 to derive two descriptive quantities. Section 6 pre-

¹Corresponding author.

Contributed by the Applied Mechanics Division of ASME for publication in the JOURNAL OF APPLIED MECHANICS. Manuscript received March 3, 2009; final manuscript received December 6, 2010; accepted manuscript posted December 8, 2010; published online April 13, 2011. Assoc. Editor: N. Sri Namachivaya.

sents a discussion of these quantities and explains how they can be combined to evaluate the behavior, and Sec. 7 gives a demonstration of their application.

2 Modal Coupling

Consider a self-adjoint, discrete, undamped structural dynamic eigenproblem. Fox and Kapoor [25] derived the eigenvalue sensitivity with respect to the parameter δ as

$$\frac{\partial \lambda_i}{\partial \delta} = \phi_i^T \left(\frac{\partial \mathbf{K}}{\partial \delta} - \lambda_i \frac{\partial \mathbf{M}}{\partial \delta} \right) \phi_i \quad (1)$$

where λ_i and ϕ_i are the eigenvalue and mass-normalized eigenvector of the i th mode, and \mathbf{M} and \mathbf{K} are the system mass and stiffness matrices. The corresponding eigenvector sensitivity is given as

$$\frac{\partial \phi_i}{\partial \delta} = -\frac{\phi_i^T \frac{\partial \mathbf{M}}{\partial \delta} \phi_i}{2} \phi_i + \sum_{r \neq i} \frac{\phi_r^T \left(\frac{\partial \mathbf{K}}{\partial \delta} - \lambda_i \frac{\partial \mathbf{M}}{\partial \delta} \right) \phi_i}{\Delta \lambda_{ir}} \phi_r \quad (2)$$

where $\Delta \lambda_{ir} = \lambda_i - \lambda_r$. Differentiating Eq. (1) with respect to δ and using Eq. (2) yield

$$\begin{aligned} \frac{\partial^2 \lambda_i}{\partial \delta^2} = & \phi_i^T \left(\frac{\partial^2 \mathbf{K}}{\partial \delta^2} - \lambda_i \frac{\partial^2 \mathbf{M}}{\partial \delta^2} - 2 \frac{\partial \lambda_i}{\partial \delta} \frac{\partial \mathbf{M}}{\partial \delta} \right) \phi_i \\ & + 2 \sum_{r \neq i} \frac{\left[\phi_r^T \left(\frac{\partial \mathbf{K}}{\partial \delta} - \lambda_i \frac{\partial \mathbf{M}}{\partial \delta} \right) \phi_i \right]^2}{\Delta \lambda_{ir}} \end{aligned} \quad (3)$$

Equation (3) gives the second derivative, or curvature, of the eigenvalue. If the i th and j th eigenvalues become close such that $\Delta \lambda_{ij}$ is very small, then the expression for curvature is dominated by the corresponding term in the summation where $r=j$, and it is this term that is responsible for the veering of the eigenvalue loci. The numerator of that term is $2[\phi_j^T((\partial \mathbf{K}/\partial \delta) - \lambda_i(\partial \mathbf{M}/\partial \delta))\phi_i]^2$, which is analogous to the coupling factor of Perkins and Mote [16]. For the purposes of this paper, the modal coupling shall be defined slightly differently as

$$\kappa_{ij} = \phi_j^T \left(\frac{\partial \mathbf{K}}{\partial \delta} - \lambda_i \frac{\partial \mathbf{M}}{\partial \delta} \right) \phi_i \quad (4)$$

Expanding this to the full set of modes, a sensitivity matrix can be defined as follows:

$$\Sigma = \Phi^T \frac{\partial \mathbf{K}}{\partial \delta} \Phi - \Phi^T \frac{\partial \mathbf{M}}{\partial \delta} \Phi \Lambda \quad (5)$$

where Φ is the complete matrix of eigenvectors $[\phi_1 \ \phi_2 \ \dots \ \phi_N]$ and Λ is a diagonal matrix of eigenvalues. The diagonal terms in Σ are the eigenvalue sensitivities and the off-diagonal terms are the modal coupling. The latter can be interpreted as cross-sensitivities, quantifying the contribution of each mode to the curvature and eigenvector derivatives of the others. For an undamped system, eigenvalue curve veering will be present wherever two modes intersect, except in the physically improbable case of the cross-sensitivities for those modes being exactly zero. In addition, because of the squaring of the modal coupling term in Eq. (3) and the opposing signs of $\Delta \lambda_{ij}$ and $\Delta \lambda_{ji}$, the two eigenvalues will always veer away from one another.

3 Eigenvector Rotation

For proximate modes i and j , if $|\Delta \lambda_{ij}| \ll |\Delta \lambda_{ir}|$ for all $r \neq i, j$, then Eq. (2) can be approximated by

$$\frac{\partial \phi_i}{\partial \delta} \approx -\frac{\phi_i^T \frac{\partial \mathbf{M}}{\partial \delta} \phi_i}{2} \phi_i + \frac{\kappa_{ij}}{\Delta \lambda_{ij}} \phi_j \quad (6)$$

From this equation (and the equivalent expression for $\partial \phi_j / \partial \delta$), it is seen that the two vectors throughout veering can always be represented by a linear combination of a single pair of vectors; as they transform, they always remain in the same plane or subspace.

Suppose that a constant matrix \mathbf{A} can be found such that $\Psi_{ij}^T \mathbf{A} \Psi_{ij} = \mathbf{I}$ for all values of δ , where \mathbf{I} is an identity matrix and Ψ_{ij} is the $N \times 2$ matrix of \mathbf{A} -normalized eigenvectors $[\psi_i \ \psi_j]$. In this case, the two eigenvectors will always form an orthonormal basis with respect to \mathbf{A} , and their magnitude and orientation within the subspace can be defined relative to a set of reference eigenvectors by a single angle. Any two eigenvalue pairs in the subspace can then be related by a rotational transformation such that

$$\Psi_{ik}^{(2)} = \Psi_{ik}^{(1)} \mathbf{T}, \quad \mathbf{T} = \begin{bmatrix} \cos(\Delta \alpha) & \sin(\Delta \alpha) \\ -\sin(\Delta \alpha) & \cos(\Delta \alpha) \end{bmatrix}, \quad \Delta \alpha = \alpha^{(1)} - \alpha^{(2)} \quad (7)$$

Here, and henceforth, bracketed superscripts denote quantities corresponding with a specific value of the parameter δ . Thus, $\lambda_i^{(n)}$, $\Psi_{ik}^{(n)}$, and any other modal properties with the superscript (n) correspond with the specific condition $\delta = \delta^{(n)}$. The absolute values of the two angles $\alpha^{(1)}$ and $\alpha^{(2)}$ have deliberately been left arbitrary; a suitable choice for the datum is examined in Sec. 4.

Equation (7) is a generalization of the simple system described by Balmès [11], and demonstrates that his observations may be extrapolated to a large class of veering systems, contingent on the existence of an appropriate orthonormalizing matrix and satisfactory agreement with Eq. (6). The latter occurs wherever two modes approach closely. The former is achieved most readily by keeping either the mass or the stiffness matrix constant, and these two scenarios will be considered in the sections that follow.

4 Cross-Sensitivity Quotient

In this section, the variation of the modal coupling throughout veering is investigated. A reduced sensitivity matrix for modes i and j shall be defined as

$$\Sigma_{ij} = \Phi_{ij}^T \frac{\partial \mathbf{K}}{\partial \delta} \Phi_{ij} - \Phi_{ij}^T \frac{\partial \mathbf{M}}{\partial \delta} \Phi_{ij} \Lambda_{ij} = \begin{bmatrix} \sigma_i & \kappa_{ji} \\ \kappa_{ij} & \sigma_j \end{bmatrix} \quad (8)$$

where σ_i is an equivalent expression for the eigenvalue sensitivity $\partial \lambda_i / \partial \delta$. The case of stiffness variation and that of mass variation will be treated separately.

4.1 Stiffness Variation. Considering a linear variation in the stiffness matrix, the mass matrix remains constant and serves as an orthonormalizing matrix, allowing the substitution of Eq. (7) in Eq. (8) using $\Psi_{ij} = \Phi_{ij}$. Noting that $\partial \mathbf{M} / \partial \delta = 0$ and using the notation $\partial \mathbf{K} / \partial \delta^{(1)} = \partial \mathbf{K} / \partial \delta^{(2)} = \mathbf{K}'$, this substitution produces

$$\Sigma_{ij}^{(2)} = \mathbf{T}^T \Phi_{ij}^{(1)T} \mathbf{K}' \Phi_{ij}^{(1)} \mathbf{T} = \mathbf{T}^T \Sigma_{ij}^{(1)} \mathbf{T} \quad (9)$$

$\Sigma_{ij}^{(2)}$ is a symmetric 2×2 matrix in which the off-diagonal elements are equal as follows:

$$\begin{aligned} \kappa_{ij}^{(2)} &= \kappa_{ji}^{(2)} \\ &= \kappa_{ij}^{(1)} [\cos^2(\Delta \alpha) - \sin^2(\Delta \alpha)] - [\sigma_j^{(1)} - \sigma_i^{(1)}] \cos(\Delta \alpha) \sin(\Delta \alpha) \\ &= \kappa_{ij}^{(0)} \cos(2\beta - 2\Delta \alpha) \end{aligned} \quad (10)$$

where

$$\tan(2\beta) = \Delta \sigma_{ji}^{(1)} / 2\kappa_{ij}^{(1)} \quad (11)$$

$$\kappa_{ij}^{(0)2} = \kappa_{ij}^{(1)2} + (\Delta\sigma_{ji}/2)^2 \quad (12)$$

and $\Delta\sigma_{ji} = \sigma_j - \sigma_i$. Keeping $\alpha^{(1)}$ constant as $\alpha^{(2)}$ changes, the corresponding modal coupling $\kappa_{ij}^{(2)}$ is seen to vary harmonically with the orientation of the vectors. The maximum coupling is given by Eq. (12) and this is used to define a corresponding set of reference vectors $\Phi_{ij}^{(0)}$ where $\alpha^{(0)} = 0$. Letting $\alpha^{(2)} = 0$ gives $\kappa_{ij}^{(2)} = \kappa_{ij}^{(0)}$ and hence from Eq. (10), $\beta = \alpha^{(1)}$. From Eq. (11), however, β is independent of $\alpha^{(2)}$ and depends only on $\alpha^{(1)}$ so that

$$\beta \equiv \alpha^{(1)}, \quad \forall \alpha^{(2)} \quad (13)$$

The angle β describes the angle between $\Phi_{ij}^{(0)}$ and $\Phi_{ij}^{(1)}$. Now, setting $\alpha^{(2)} = \alpha^{(1)}$, the superscripts (1) and (2) are equivalent and can be omitted so that Eqs. (10)–(12) become

$$\kappa_{ij} = \kappa_{ij}^{(0)} \cos(2\beta) \quad (14)$$

$$\Delta\sigma_{ji}/2 = \kappa_{ij}^{(0)} \sin(2\beta) \quad (15)$$

$$\kappa_{ij}^{(0)2} = \kappa_{ij}^2 + (\Delta\sigma_{ji}/2)^2 \quad (16)$$

and the eigenvector transformation is given by

$$\Phi_{ij} = \Phi_{ij}^{(0)} \mathbf{T}, \quad \mathbf{T} = \begin{bmatrix} \cos \beta & \sin \beta \\ -\sin \beta & \cos \beta \end{bmatrix} \quad (17)$$

From Eq. (15), the angle β is zero when $\Delta\sigma_{ji} = 0$ and the sensitivities of the two modes are equal: effectively the point where the eigenvalue loci swap trajectories. This corresponds to the point where the eigenvalues are closest, and since Eqs. (3) and (6) can be written $\partial^2 \lambda_i / \partial \delta^2 \approx 2(\kappa_{ij}^2 / \Delta \lambda_{ij})$ and $\partial \phi_i / \partial \delta \approx (\kappa_{ij} / \Delta \lambda_{ij}) \phi_j$ for this case, it is also the point where the eigenvalue curvature and eigenvector sensitivity are greatest. The reference vectors thus form a veering datum set where the modal coupling is greatest and the intensity of the veering is strongest. It follows that the modal coupling, or cross-sensitivity, can be used to measure the local intensity of veering. This finding is in keeping with the observations of Sec. 2. Furthermore, the maximum cross-sensitivity is easily computed from the modal properties for any δ , and it is convenient to define a cross-sensitivity quotient as $\text{CSQ}_{ij} = (\kappa_{ij} / \kappa_{ij}^{(0)})^2$. Using Eqs. (14)–(16),

$$\text{CSQ}_{ij} = \cos^2(2\beta) = \frac{\kappa_{ij}^2}{\kappa_{ij}^2 + (\Delta\sigma_{ji}/2)^2} \quad (18)$$

A more general definition is afforded by examining the eigenvector rotations. As $\beta \rightarrow \pm(\pi/4)$, the modal coupling goes to zero and from Eq. (6) the vector rotation also halts. Thus, for an idealized veering case (without interaction from other modes), the datum vectors are oriented exactly half way between their asymptotic limits.

4.2 Mass Variation. Now consider a linear variation in the mass matrix with constant stiffness matrix. The stiffness matrix may be used as the orthonormalizing matrix such that

$$\Psi_{ij}^T \mathbf{K} \Psi_{ij} = \mathbf{I}, \quad \Psi_{ij} = \Phi_{ij} \Lambda_{ij}^{-(1/2)} \quad (19)$$

where Λ is a diagonal matrix so the inverse square root needs no further clarification. Combining Eqs. (8) and (19) while noting $\partial \mathbf{K} / \partial \delta = 0$ yields

$$\Sigma_{ij} = -\Lambda_{ij}^{(1/2)} \Psi_{ij}^T \frac{\partial \mathbf{M}}{\partial \delta} \Psi_{ij} \Lambda_{ij}^{(3/2)} \quad (20)$$

This matrix is not symmetric, and maximum values for κ_{ij} and κ_{ji} will not necessarily coincide. In order to define a cross-sensitivity quotient for the two modes in the same manner as before, a symmetric matrix is defined in the form of an adapted sensitivity matrix as follows:

$$\Sigma_{ij}^* = \Lambda_{ij}^{-(1/2)} \Sigma_{ij} \Lambda_{ij}^{-(3/3)} = -\Psi_{ij}^T \frac{\partial \mathbf{M}}{\partial \delta} \Psi_{ij} \quad (21)$$

Substituting Eq. (7) and again writing $\partial \mathbf{M} / \partial \delta^{(1)} = \partial \mathbf{M} / \partial \delta^{(2)} = \mathbf{M}'$,

$$\Sigma_{ij}^{*(2)} = -\mathbf{T}^T \Psi_{ij}^{(1)T} \mathbf{M}' \Psi_{ij}^{(1)} \mathbf{T} = \mathbf{T}^T \Sigma_{ij}^{*(1)} \mathbf{T} \quad (22)$$

This is equivalent to Eq. (9) and, by analogy,

$$\text{CSQ}_{ij}^* = \frac{\kappa_{ij}^{*2}}{\kappa_{ij}^{*2} + (\Delta\sigma_{ji}^*/2)^2} = \frac{\frac{\kappa_{ij}^2}{\lambda_i^3 \lambda_j}}{\left(\frac{\kappa_{ij}^2}{\lambda_i^3 \lambda_j} + \frac{1}{4} \left(\frac{\sigma_j}{\lambda_j^2} - \frac{\sigma_i}{\lambda_i^2} \right)^2 \right)} \quad (23)$$

Note that the eigenvalues are generally close at veering, and if $\lambda_i \approx \lambda_j$, then $\kappa^* \approx \kappa$ and $\text{CSQ}^* \approx \text{CSQ}$. Equations (18) and (23) are valid for any symmetric, undamped structural eigenproblem with linear variation of the mass or stiffness matrices.

5 Modal Dependence Factor

Veering is distinguished from other forms of parametric variation by the swapping of modal properties from one mode to another. This is effected by a transformation of the eigenvectors within a fixed subspace. If the vectors stray significantly outside their subspace, it is an indication that they are interacting with other modes. On this premise, a modal dependence factor (MDF) is derived below to quantify the contribution of the interaction between two modes to their total variation.

A measure of the conformity of the mass-normalized eigenvectors to their subspace is found by comparing the ℓ^2 -norms of Eqs. (2) and (6) within the normal basis defined by the complete eigenvector set as follows:

$$Q_{ij} = \sqrt{\frac{-\left(\frac{1}{2} \phi_i^T \frac{\partial \mathbf{M}}{\partial \delta} \phi_i\right)^2 + (\kappa_{ij} / \Delta \lambda_{ij})^2}{-\left(\frac{1}{2} \phi_i^T \frac{\partial \mathbf{M}}{\partial \delta} \phi_i\right)^2 + \sum_{r \neq i} (\kappa_{ir} / \Delta \lambda_{ir})^2}} \quad (24)$$

As before, considering a change in parameter δ causing a variation of the stiffness matrix such that $\partial \mathbf{M} / \partial \delta = 0$, Eq. (24) can be written

$$\text{MDF}_{ij} = Q_{ij}^2 = \frac{(\kappa_{ij} / \Delta \lambda_{ij})^2}{\sum_{r \neq i} (\kappa_{ir} / \Delta \lambda_{ir})^2} \quad (25)$$

This equation requires knowledge of the modal parameters for all the modes, but it is desirable that the modal dependence factor, as with the cross-sensitivity quotient, may be computed using only modal parameters for the two modes concerned. The eigenvector derivative $\partial \phi_i / \partial \delta$ can be obtained in a computationally efficient manner using only modal properties for the i th mode with Nelson's method [26]. Transposing Eq. (2), post-multiplying by $\mathbf{M} \phi_j$, and noting the orthogonality properties gives

$$\frac{\partial \phi_i}{\partial \delta} \mathbf{M} \phi_j = \kappa_{ij} / \Delta \lambda_{ij} \quad (26)$$

Post-multiplying Eq. (2) again, this time by $\mathbf{M}(\partial \phi_i / \partial \delta)$, and remembering $\partial \mathbf{M} / \partial \delta = 0$ gives

$$\frac{\partial \phi_i}{\partial \delta} \mathbf{M} \frac{\partial \phi_i}{\partial \delta} = \sum_{r \neq i} (\kappa_{ir} / \Delta \lambda_{ir})^2 \quad (27)$$

Combining Eqs. (25)–(27) yields

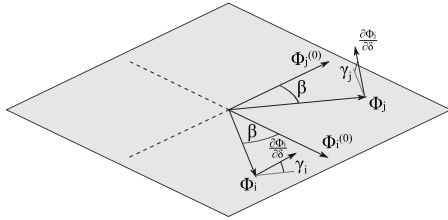


Fig. 1 A geometric interpretation of the cross-sensitivity quotient and modal dependence factors described by $CSQ_{ij} = \cos^2(2\beta)$, $MDF_{ij} = \cos^2(\gamma_i)$, and $MDF_{ji} = \cos^2(\gamma_j)$. Depicted is a plane or subspace in the normal coordinate system containing two eigenvectors ϕ_i and ϕ_j . These vectors are separated from the veering datum vectors for that subspace, $\phi_i^{(0)}$ and $\phi_j^{(0)}$, by angle β . The corresponding eigenvector derivatives are pictured forming angles γ_i and γ_j with the subspace.

$$MDF_{ij} = \frac{\left(\frac{\partial \phi_i^T \mathbf{M} \phi_j}{\partial \delta} \right)^2}{\frac{\partial \phi_i^T \mathbf{M} \phi_i}{\partial \delta} \frac{\partial \phi_j^T \mathbf{M} \phi_j}{\partial \delta}} \quad (28)$$

giving the contribution of the j th mode to the derivative of the i th eigenvector. From vector algebra and inner products, this is seen to be equivalent to the square of the cosine of the angle between the eigenvector derivative and the plane Φ_{ij} in the normal coordinate system. The same approach may be taken for mass matrix variation with $\partial \mathbf{K} / \partial \delta = 0$ to produce

$$MDF_{ij}^* = \frac{\left(\frac{\partial \psi_i^T \mathbf{K} \psi_j}{\partial \delta} \right)^2}{\frac{\partial \psi_i^T \mathbf{K} \psi_i}{\partial \delta} \frac{\partial \psi_j^T \mathbf{K} \psi_j}{\partial \delta}} \quad (29)$$

where ψ_i is once more the stiffness-normalized i th eigenvector, and careful attention must be given to the correct normalization of $\partial \psi_i / \partial \delta$ when using Nelson's scheme.

In the case of several modes veering simultaneously, the MDFs may be summed to quantify the confinement of a vector within the larger subspace. For the two mode scenario, the MDFs quantify the validity of Eq. (6) and thus the quality of the assumptions made in the derivation of the CSQ.

6 Veering Index

Veering has been shown to occur in the presence of strong modal coupling and proximate modes. Contrarily, subjective observations of the behavior are most often made in systems with weak modal coupling outside of the veering regions. In these circumstances the eigenvalues must be close to induce veering, producing more rapid and hence more discernible instances of the effect.

The difficulty in quantifying the behavior lies in determining what values constitute strong modal coupling and close eigenvalues. A better definition is afforded by considering the modal interactions in the context of the complete system; to produce veering, the two modes must be close *with respect to their coupling*, and they must be isolated from the influence of other modes. These two requirements are quantified with the CSQ and the MDF, respectively. It is necessary and sufficient that they are both close to unity to produce veering.

A geometric interpretation is given in Fig. 1. From this the MDFs are seen to describe the extent to which the eigenvector derivatives deviate from their subspace, while the CSQ describes their orientation relative to the veering datum within that subspace. Thus, the MDFs determine whether the modes *will* veer, and on this presumption the CSQ determines whether they *are* veering.

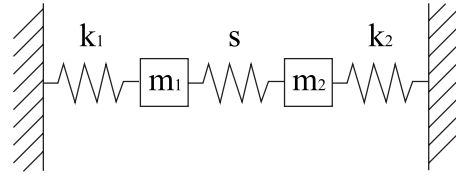


Fig. 2 Two degree of freedom spring-mass system with light spring coupling s between the masses

A veering index is proposed as the product of the CSQ and the two MDFs as follows:

$$VI_{ij} = MDF_{ij} \times CSQ_{ij} \times MDF_{ji} \quad (30)$$

$$VI_{ij}^* = MDF_{ij}^* \times CSQ_{ij}^* \times MDF_{ji}^* \quad (31)$$

This index provides an unambiguous measure of the extent to which two modes are swapping properties with each other. It is a definitive indicator for the presence of veering between two modes, based not upon subjective observations but on physically relevant manifestations.

7 Examples

Three examples are presented here. The first is a simple two degree of freedom (DOF) system which will demonstrate the principles of the cross-sensitivity quotient. The second is a four DOF system which has been chosen to demonstrate some of the more surprising results obtained with the veering index. The third and final example is a finite element (FE) discretization of a cantilever plate, showing how the indices perform on a more typical physical representation of a system.

7.1 Two DOF Example. Figure 2 shows a simple two DOF arrangement, consisting of two grounded spring-mass systems with a light coupling spring between them. In this example, $k_1 = k_2 \gg s$. Away from veering, each mass dominates the motion for its respective vibration mode. As m_2 varies, the natural frequencies of the two modes converge and veer, forming two symmetrical mode shapes where $m_2 = m_1$. The eigenvalue loci are plotted in Fig. 3(a). Because there are only two modes in this system, the modal dependence factors MDF_{12} and MDF_{21} will always be unity. In this case, the cross-sensitivity quotient and the veering index are identical and are plotted using Eq. (23) in Fig. 3(b). The index provides a clear indication of the intensity of veering, corresponding with the behavior observed in the eigenvalue plot. The “half-CSQ parameter bandwidth” has been marked, denoting the region within which the CSQ exceeds 0.5. The effect of veering on the eigenvalue loci is most pronounced in this range.

7.2 Four DOF Example. The second example is illustrated in Fig. 4. It consists of two pairs of lightly coupled spring-mass systems, as used in the first example, with an even lighter spring coupling the two systems together. The masses are all equal in this example and the parameter change δ corresponds to a linear increase in the stiffnesses of k_1 and k_2 . The initial spring stiffnesses k_{1-4} are chosen such that prior to veering, modes 1–4 are dominated by the motion of DOFs 1–4, respectively, and the coupling springs s_{1-3} introduce light modal coupling where $s_1 = s_2 \gg s_3$. With this arrangement, it is expected that mode 1 will be closely coupled to mode 3 and that mode 2 will be closely coupled to mode 4. Modes 1 and 4 may be lightly coupled while modes 2 and 3 should experience the least coupling. The eigenvalues are plotted in Fig. 5(a), where on first inspection modes 2 and 3 appear to veer away from each other. In fact the observed veering is caused by the concurrent interaction of mode pairs 1–3 and 2–4, and this is clearly indicated by the veering indices in Fig. 5(b). The only curves to rise substantially above zero in this plot are those corresponding to VI_{13} and VI_{24} . Examining the cross-sensitivity quo-

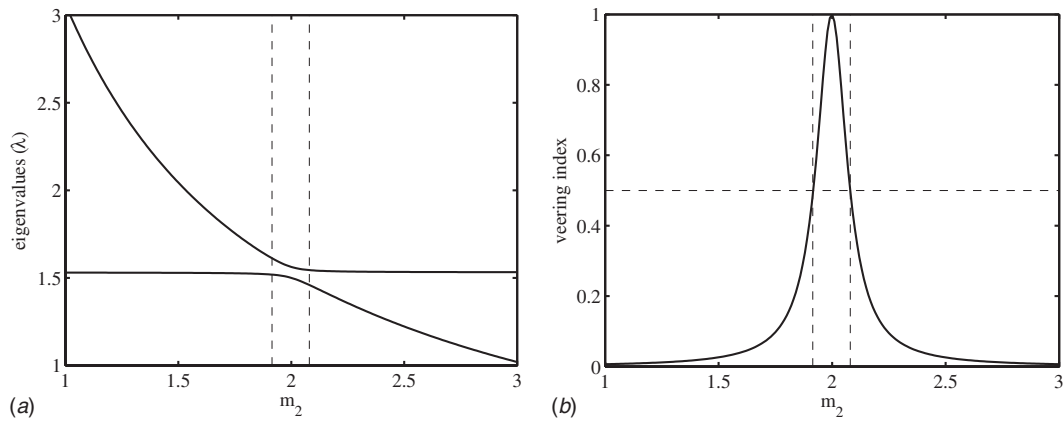


Fig. 3 Two DOF system plotted for $k_1=k_2=3$, $m_1=2$, $s=0.0625$, and $m_2=1\dots3$. Dotted lines indicate the half-CSQ parameter bandwidth.

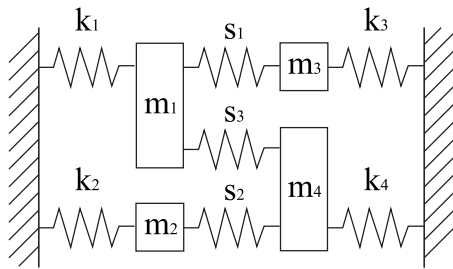


Fig. 4 Four degree of freedom spring-mass system with light spring couplings s_{1-3} between the masses

tients in Fig. 5(c) shows that as the two mode pairs veer, the vectors swing close to the veering datums for other mode pair combinations; the sharp peaks at $\delta \approx 77$ correspond to pairs 2–3 and 1–4. Consultation of the modal dependence factors in Fig. 5(d), however, confirms that while the factors for the veering mode pairs stay close to unity, those for the spurious mode combinations remain small, ensuring a true representation of the modal transformations in the veering index.

Increasing the coupling between the two spring-mass systems so that $s_3=s_2=s_1$ produces similar eigenvalue loci, as presented in Fig. 6(a). Referring to the veering indices in Fig. 6(b), however, reveals that the observed curvature is now attributable to the in-

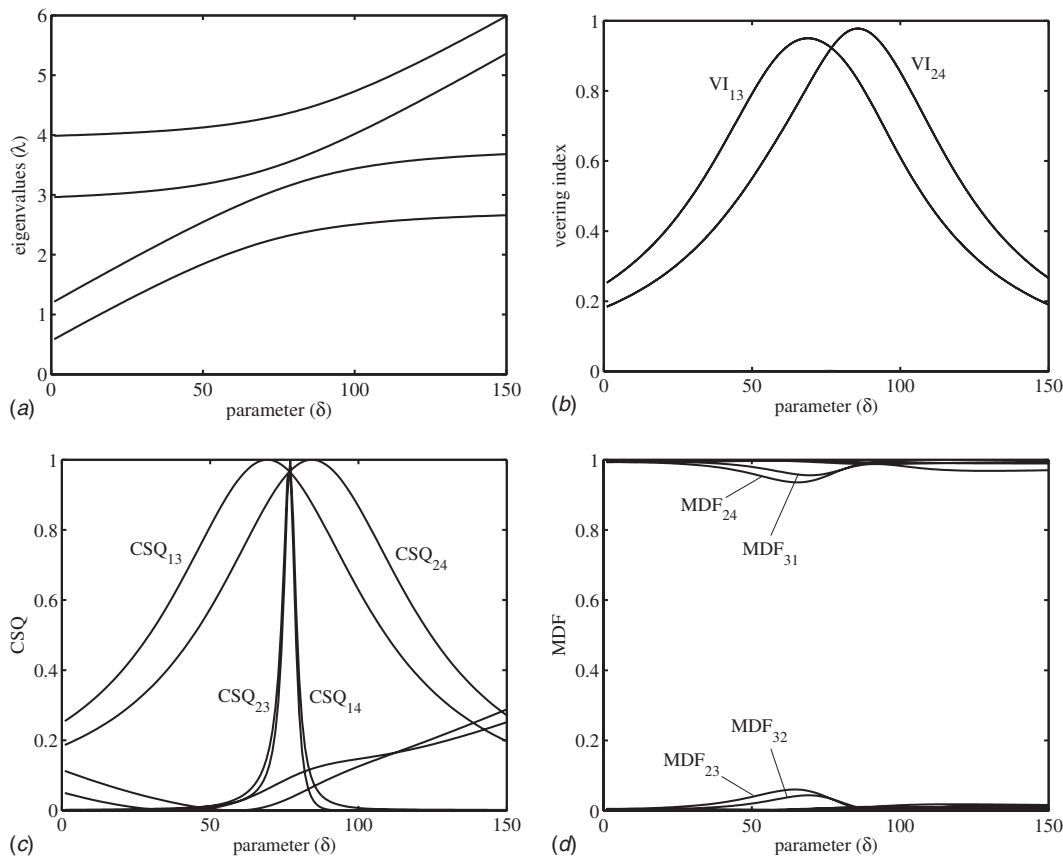


Fig. 5 Four DOF system plotted for $m_1=m_2=m_3=m_4=1$, $s_1=s_2=0.6$, $s_3=0.05$, $k_1=0.1+0.03\delta$, $k_2=0.75+0.03\delta$, $k_3=2.2$, $k_4=3.2$, and $\delta=1\dots150$

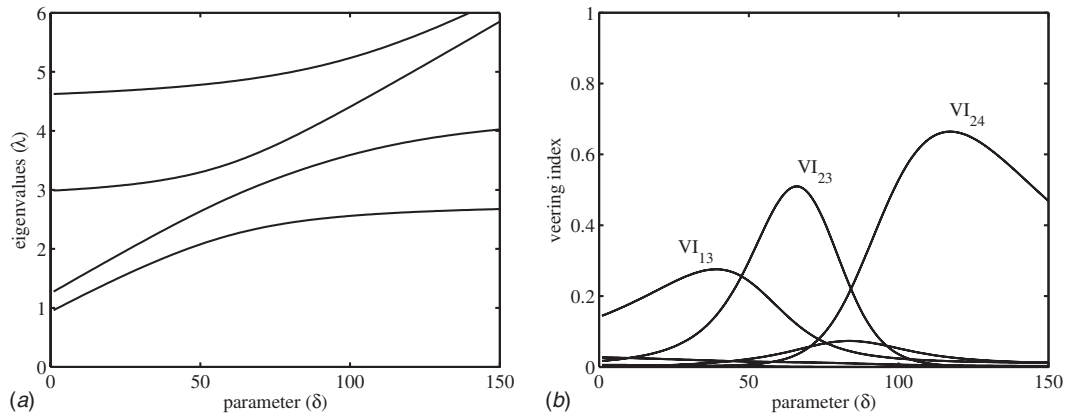


Fig. 6 The four DOF system plotted for $s_1=s_2=s_3=0.6$

interaction of several mode pairs, in three distinct phases. First modes 1 and 3 begin to veer. As mode 3 takes on the properties of mode 1, its coupling to mode 2 increases. At the same time, the 2nd and 3rd eigenvalues get closer and the combination of these effects causes those two modes to veer, taking the dominant role in the variation. As these modes diverge again, the 2nd mode starts to veer with the 4th and the corresponding veering index peaks. At no stage are any two modes interacting solely with one

another and this is witnessed by the veering indices which are always significantly below unity. The practical implications of the low veering indices are manifested as a more generalized transformation of the eigenvectors spanning the full subspace.

7.3 Cantilever Plate Example. The third example examines a more realistic physical system in the form of a rectangular cantilever plate. The FE simulation employs thin plate approximations and only bending is considered, using three degrees of freedom at each node, as described by Warburton [27]. The plate is comprised of 400 rectangular isotropic plate elements, forming a 20×20 grid. The system has 1323 DOFs. The nodes at the root of the cantilever are fully constrained in translation and both rotational DOFs.

The parameter to be varied is the aspect ratio of the plate. The depth of the plate, denoted b and defined as the distance between the root and the free edge, takes a constant value of 0.1 m. The width of the plate, denoted a and defined as the distance between the two opposing free edges, is varied between 0.05 m and 0.15 m. The thickness of the plate stays constant at 1 mm. The material properties are chosen to simulate a generic steel, with a Young's modulus of 200 GPa, a density of 7800 kg m^{-3} , and a Poisson's ratio of 0.3.

This example differs from the previous two examples in that the parameter affects both the mass *and* stiffness matrices simultaneously. This condition violates the assumptions made in the derivation of the veering indices. The approach taken here is to treat the mass and stiffness modifications as two independent parameters for the purposes of calculating the indices; it is expected that the modal coupling will generally be dominated by one or other of

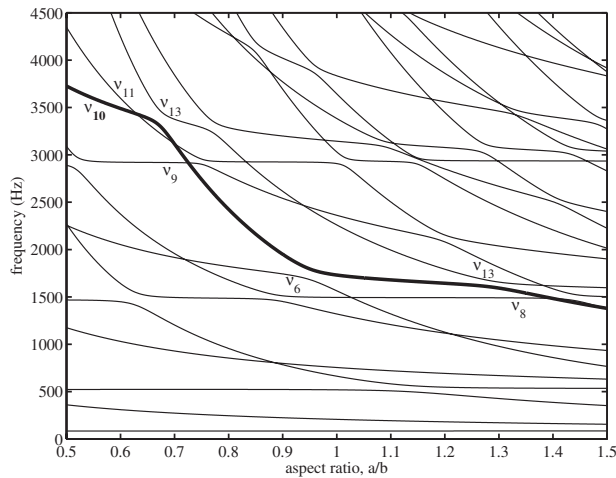


Fig. 7 Natural frequencies for the cantilever plate

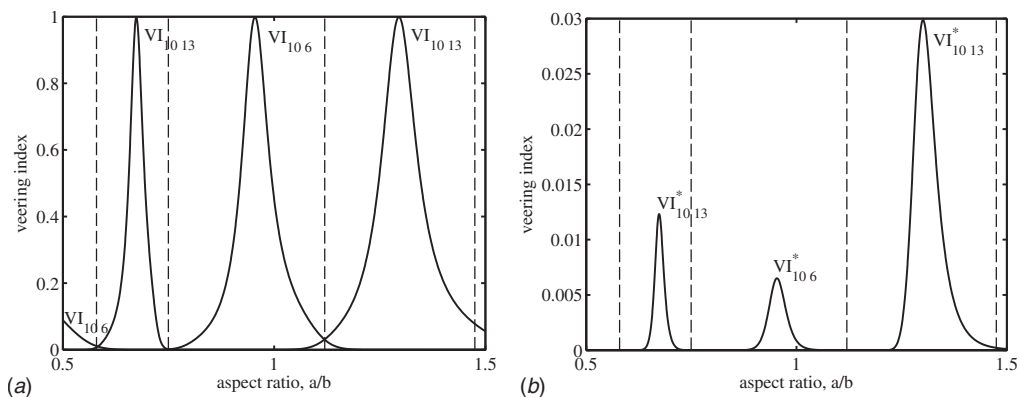


Fig. 8 Veering indices for the cantilever plate with respect to (a) the change in stiffness, and (b) the change in mass. Note the different scaling of the ordinate axes. Dashed lines correspond with the mode shapes in Fig. 9.

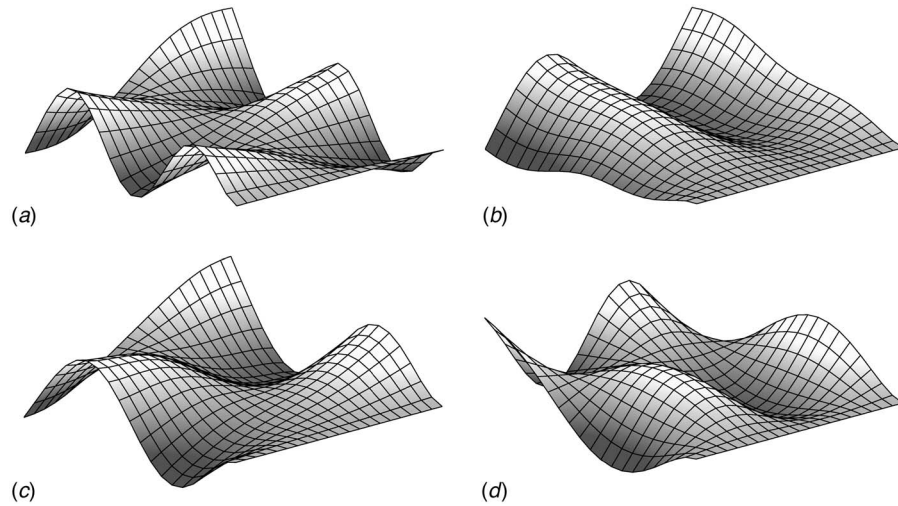


Fig. 9 Mode shapes for the tenth mode of the isotropic plate, with aspect ratios a/b of (a) 0.58, (b) 0.75, (c) 1.12, and (d) 1.475. The cantilever root is along the bottom right edge in these diagrams.

these parameters, and the respective index will offer meaningful indications of the state of veering.

A further consequence of the choice of parameter is a nonlinear dependence in both the mass and stiffness matrices. In computing the veering indices for a given parameter value, the matrix variations are effectively linearized about that point. Thus, reasonable results can be expected in the vicinity of the veering datum but the accuracy would be expected to drop off away from this point. This shortcoming does not necessarily impinge significantly on the applicability of the indices and it should be noted that it only affects the CSQ; the geometric interpretation of the MDF is not affected by nonlinearity.

The first 24 natural frequencies computed by the FE code, $\nu_1 - \nu_{24}$, are shown in Fig. 7. They are numbered in the order of ascending frequency at the left edge of the figure (where $a/b = 0.5$) and they retain their numbering for all values of a/b , producing some misleading results in the visible range of the graph where, for example, $\nu_{13} < \nu_{12}$. The figure shows regions of high modal density, and while some modes are clearly seen to veer, others appear to cross. The tenth frequency locus, highlighted as the bold line in Fig. 7, is taken as an example. On the left of the figure, it veers with mode 13 while crossing the loci of modes 9 and 11. In the center of the figure, it veers with mode 6, before continuing to veer again with mode 13 on the right edge of the figure. Before leaving the graph, it passes through the locus of mode 8 twice, where mode 8 is itself in the process of veering with mode 9.

The veering indices for mode 10, $VI_{10,1} - VI_{10,24}$, are plotted in Fig. 8 with respect to both the mass and the stiffness variation. The only curves which can be seen rising above zero are those corresponding with the 6th and 13th modes, supporting the observations of veering in the frequency loci. It is also apparent that the stiffness plays the dominant role in the veering of the frequency curves; the indices for the stiffness parameter almost reach unity, in contrast to those for the mass parameter which never rise above 0.03. In situations such as this, where either the mass or stiffness matrix dominates, Eq. (30) can be used with the full, simultaneous mass and stiffness variation to produce a good approximation to the relevant veering index. As noted at the end of Sec. 4, the disparity between the CSQs in Eqs. (18) and (23) is small where the eigenvalues are close. Accordingly, as with the effects of nonlinearity, the information derived in the veering region remains pertinent. Outside of the veering region, the MDF ensures that the value of the index is small.

Where mode 10 veers, its mode shape transitions to those of the modes it veers with. Figure 9 shows the four stages of the progression of the mode shape, with the corresponding aspect ratios indicated as dashed lines in Fig. 8. In the range studied, the frequency locus of mode 10 also crosses those of four apparently uncoupled modes, and their mode shapes are shown in Fig. 10. At several crossing points, these modes are themselves in the process of veering with one another; the mode shapes presented are not from the exact crossing points but are instead the “clean” modes sampled from nearby points, together representing the full subspace of the uncoupled modes. It is interesting to note that the mode shapes for mode 10 are all antisymmetric, while the uncoupled mode shapes are all symmetric. These results support previous observations [2,16,28] that a symmetric mode’s frequency locus will always cross that of an antisymmetric mode while two symmetric modes or two antisymmetric modes will generally veer.

8 Conclusions

Three new criteria have been derived to describe the modal interactions in eigenvalue curve veering. The *cross-sensitivity quotient* describes the state of veering of two modes within their subspace, the *modal dependence factor* identifies the conformity of the modes to that subspace, and the *veering index* combines the two to give a definitive quantification of the intensity of veering.

Three examples have been included to demonstrate the performance of the indices under different conditions. An important feature of the technique is that it requires only knowledge of the modal properties for the two modes concerned, and at only a single parameter value. The normalized values computed with these expressions provide unambiguous measures of the physical properties responsible for the behavior. Although the results are insightful when considered in isolation, their principal application is expected to be in the interpretation and extrapolation of less esoteric quantities.

The techniques are currently limited to linear variations of the mass or stiffness matrices. It is hoped that future work will produce more general expressions. Nonetheless, the veering indices presented here have been shown to produce useful results for a simultaneous nonlinear variation of the mass and stiffness matrices despite a lack of mathematical rigor in this case.

To the best of the authors’ knowledge, the methods derived here offer the first objective numerical quantification of veering. The

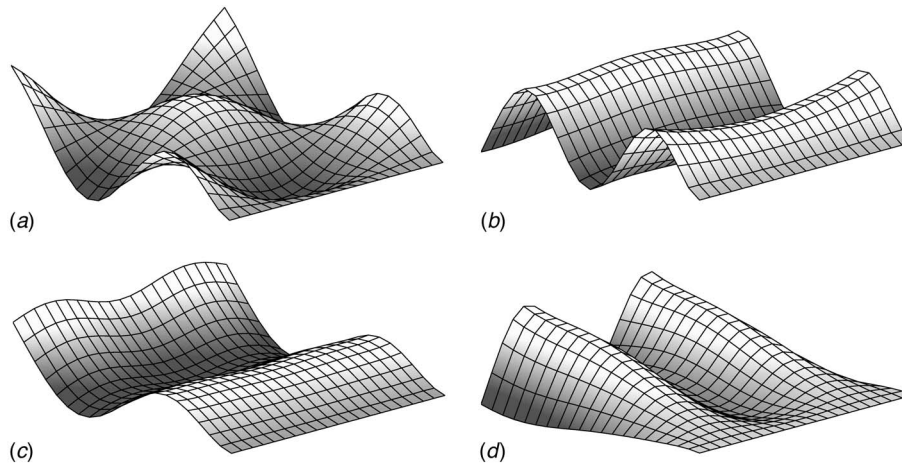


Fig. 10 Mode shapes for the uncoupled modes where they cross the tenth mode of the isotropic plate: (a) mode 11, (b) mode 9, (c) mode 8 (pre-veering) and (d) mode 8 (post-veering). The cantilever root is along the bottom right edge in these diagrams.

techniques are expected to find application in a wide range of parametric studies and provide a basis for the development of advanced analytical tools in fields such as model updating, damage detection, response suppression, and stability analysis.

References

- [1] Claassen, R. W., and Thorne, C. J., 1962, "Vibrations of a Rectangular Cantilever Plate," *J. Aerosp. Sci.*, **29**(11), pp. 1300–1305.
- [2] Webster, J. J., 1968, "Free Vibrations of Rectangular Curved Panels," *Int. J. Mech. Sci.*, **10**, pp. 571–582.
- [3] du Bois, J. L., Adhikari, S., and Lieven, N. A. J., 2007, "Experimental and Numerical Investigation of Mode Veering in a Stressed Structure," *Proceedings of the 25th International Modal Analysis Conference*, Vol. 25, p. 233.
- [4] du Bois, J. L., Adhikari, S., and Lieven, N. A. J., 2009, "Eigenvalue Curve Veering in Stressed Structures: An Experimental Study," *J. Sound Vib.*, **322**, pp. 1117–1124.
- [5] McIntyre, M. E., and Woodhouse, J., 1988, "On Measuring the Elastic and Damping Constants of Orthotropic Sheet Materials," *Acta Metall.*, **36**(6), pp. 1397–1416.
- [6] Hodges, C. H., 1982, "Confinement of Vibration by Structural Irregularity," *J. Sound Vib.*, **82**, pp. 411–424.
- [7] Hodges, C. H., and Woodhouse, J., 1983, "Vibration Isolation From Irregularity in a Nearly Periodic Structure: Theory and Measurements," *J. Acoust. Soc. Am.*, **74**(3), pp. 894–905.
- [8] Pierre, C., and Dowell, E. H., 1987, "Localization of Vibrations by Structural Irregularity," *J. Sound Vib.*, **114**(3), pp. 549–564.
- [9] Pierre, C., 1988, "Mode Localization and Eigenvalue Loci Veering Phenomena in Disordered Structures," *J. Sound Vib.*, **126**(3), pp. 485–502.
- [10] Afolabi, D., and Mehmed, O., 1994, "On Curve Veering and Flutter of Rotating Blades," *ASME J. Eng. Gas Turbines Power*, **116**, pp. 702–708.
- [11] Balmès, E., 1993, "High Modal Density, Curve Veering, Localization: A Different Perspective on the Structural Response," *J. Sound Vib.*, **161**(2), pp. 358–363.
- [12] Benedettini, F., Zulli, D., and Alaggio, R., 2009, "Frequency-Veering and Mode Hybridization in Arch Bridges," *Proceedings of the 27th International Modal Analysis Conference*.
- [13] Igusa, T., 1993, "Critical Configurations of Systems Subjected to Wide-Band Input," *J. Sound Vib.*, **168**(3), pp. 525–541.
- [14] Adhikari, S., and Friswell, M. I., 2007, "Random Matrix Eigenvalue Problems in Structural Dynamics," *Int. J. Numer. Methods Eng.*, **69**(3), pp. 562–591.
- [15] Adhikari, S., 2007, "Joint Statistics of Natural Frequencies of Stochastic Dynamic Systems," *Comput. Mech.*, **40**(4), pp. 739–752.
- [16] Perkins, N. C., and Mote, C. D., Jr., 1986, "Comments on Curve Veering in Eigenvalue Problems," *J. Sound Vib.*, **106**(3), pp. 451–463.
- [17] Triantafyllou, M. S., and Triantafyllou, G. S., 1991, "Frequency Coalescence and Mode Localisation Phenomena: A Geometric Theory," *J. Sound Vib.*, **150**(3), pp. 485–500.
- [18] Afolabi, D., 1991, "Modal Interaction in Linear Dynamic Systems Near Degenerate Modes," NASA Technical Memorandum Report No. 105315.
- [19] Seyranian, A., and Mailybaev, A., 2003, "Interaction of Eigenvalues in Multi-Parameter Problems," *J. Sound Vib.*, **267**(5), pp. 1047–1064.
- [20] Seyranian, A. P., Kirillov, O. N., and Mailybaev, A. A., 2005, "Coupling of Eigenvalues of Complex Matrices at Diabolic and Exceptional Points," *J. Phys. A*, **38**(8), pp. 1723–1740.
- [21] Kirillov, O., Mailybaev, A., and Seyranian, A., 2005, "Unfolding of Eigenvalue Surfaces Near a Diabolic Point," *J. Phys. A*, **38**, pp. 5531–5546.
- [22] Seyranian, A., Lund, E., and Olhoff, N., 1994, "Multiple Eigenvalues in Structural Optimization Problems," *Struct. Multidiscip. Optim.*, **8**(4), pp. 207–227.
- [23] Altintas, G., 2009, "Effect of Mass Based Imperfections on Behavior of Linear Vibrating Plates Near Degenerate Modes," *J. Vib. Control*, **15**(2), pp. 219–231.
- [24] Liu, X. L., 2002, "Behaviour of Derivatives of Eigenvalues and Eigenvectors in Curve Veering and Mode Localisation and Their Relation to Close Eigenvalues," *J. Sound Vib.*, **256**(3), pp. 551–564.
- [25] Fox, R. L., and Kapoor, M. P., 1968, "Rates of Change of Eigenvalues and Eigenvectors," *AIAA J.*, **6**(12), pp. 2426–2429.
- [26] Nelson, R. B., 1976, "Simplified Calculation of Eigenvector Derivatives," *AIAA J.*, **14**(9), pp. 1201–1205.
- [27] Warburton, G. B., 1976, *The Dynamical Behaviour of Structures*, 2nd ed., Pergamon, Oxford/New York.
- [28] Nair, P. S., and Durvasula, S., 1973, "On Quasi-Degeneracies in Plate Vibration Problems," *Int. J. Mech. Sci.*, **15**, pp. 975–986.